Cell Reports
Physical Science

CellPress
OPEN ACCESS

Report

Selective deactivation of perovskite grain boundaries

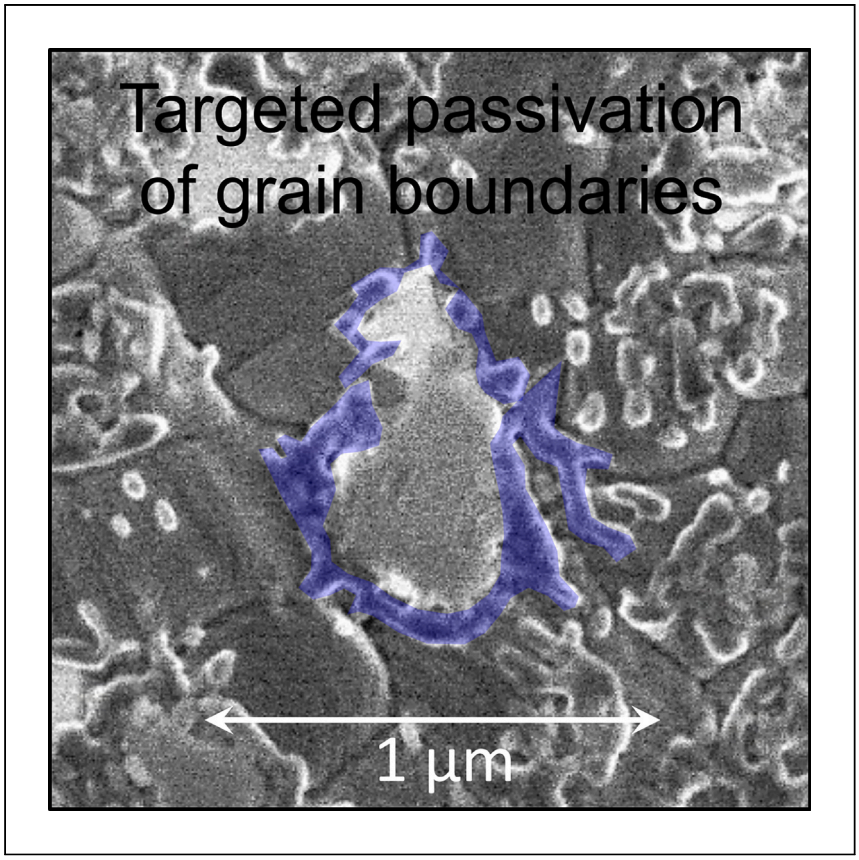

Awais et al. report the use of biphenyl-containing ligands for selective deactivation of grain boundaries on perovskite films. Corresponding solar cells demonstrate improved performance in efficiency and stability.

Muhammad Awais, Soumya Kundu, Dongyang Zhang, ..., Sergey Dayneko, Furui Tan, Makhsud I. Saidaminov

msaidaminov@uvic.ca

Highlights

Biphenyl-containing ligand is used to passivate the surface of perovskite films

The ligand selectively reacts with lead iodide and covers grain boundaries

Such-passivated solar cells demonstrate enhanced stability against water

Awais et al., Cell Reports Physical Science 4, 101634
October 18, 2023
https://doi.org/10.1016/j.xcrp.2023.101634

Cell Reports
Physical Science

CellPress
OPEN ACCESS

Report

Selective deactivation of perovskite grain boundaries

Muhammad Awais,[1,6] Soumya Kundu,[2,6] Dongyang Zhang,[2] Vishal Yeddu,[2] Mohammad Reza Kokaba,[1] Yameen Ahmed,[1] Wen Zhou,[3] Sergey Dayneko,[2] Furui Tan,[4] and Makhsud I. Saidaminov[1,2,5,7,*]

SUMMARY

Grain boundaries in perovskites are a major source of degradation in perovskite solar cells. Here, we report selective passivation of perovskite grain boundaries with the aid of biphenyl-containing moieties. We find that biphenyl ligands selectively react with PbI_2-rich interfaces but not with perovskite itself. Such targeted defect deactivation of grain boundaries leads to extended radiative recombination lifetime from 1 to 2.7 μs while allowing for efficient charge transfer from grains. The hydrophobic nature of benzene ring present in biphenyl improves the stability of perovskite in direct reaction with water by a factor of 3. The devices, all fabricated in ambient air, show significantly improved reproducibility (17%–21% efficiency) and increased open-circuit voltage of 1.11 V. This work offers a design principle for selective passivation of grain boundaries and chemical stabilization of hybrid structures.

INTRODUCTION

Perovskite solar cells (PSCs) surpassed 25% power conversion efficiency (PCE) in the lab and are now at the cusp of commercialization.[1–12] Perovskites provide a range of desirable optoelectronic properties, including band gap tunability and long charge carrier lifetime.[13–17] A major challenge in the development of PSCs has been their instability against moisture and oxygen, which lead to the decay of their performance much faster than what the stability standards demand.[18–22]

Following the gradual move from $MAPbI_3$ (MA stands for methylammonium, $CH_3NH_3^+$) to $FAPbI_3$ (FA stands for formamidinium, $HC(NH_2)^+$) as a light absorber layer, many important studies improved the stability of PSCs.[23–29] For example, Seok et al. demonstrated compositional engineering of PSCs and incorporated $MAPbBr_3$ into $FAPbI_3$ to stabilize the perovskite phase.[30,31] You et al. introduced organic halide salt, phenethylammonium iodide (PEAI), and Huang et al. introduced quaternary ammonium halides for defect passivation or interface engineering.[32,33] Grätzel et al. tailored the morphology and structure of the perovskite absorber layer by phosphonic acid ammonium additives, which act as a cross-linker between neighboring grains.[34,35]

It is well established that grain boundaries (GBs) in perovskites are a major source of degradation in PSCs.[36] This is because GBs have a higher density of defects and impurities, making them thermodynamically more reactive than the bulk material. When PSCs are exposed to stressors such as moisture, light, bias, or high temperature, GBs tend to break first, leading to the overall degradation of the device.[37,38] For example, methylammonium cations can be deprotonated by water molecules

[1]Department of Electrical & Computer Engineering, University of Victoria, 3800 Finnerty Road, Victoria, BC V8P 5C2, Canada

[2]Department of Chemistry, University of Victoria, 3800 Finnerty Road, Victoria, BC V8P 5C2, Canada

[3]Department of Chemistry, University of Calgary, 2500 University Drive NW, Calgary, AB T2N 1N4, Canada

[4]Key Laboratory of Photovoltaic Materials, Henan University, Kaifeng, Henan 475004, P.R. China

[5]Centre for Advanced Materials and Related Technologies (CAMTEC), University of Victoria, 3800 Finnerty Road, Victoria, BC V8P 5C2, Canada

[6]These authors contributed equally

[7]Lead contact

*Correspondence: msaidaminov@uvic.ca

https://doi.org/10.1016/j.xcrp.2023.101634

that are easily penetrated into GBs or by superoxide anions that are formed due to the transfer of electron from photoexcited perovskite.[39,40]

The conventional approach for surface passivation of perovskites is to incorporate low-dimensional structures, predominantly with the aid of PEAI. While effective at time-zero, these low-dimensional perovskites tend to react with underlying perovskite under external stimuli. In addition, they are unselective to GBs only: they cover all surfaces, potentially impeding charge carrier collection from the grains. Therefore, there is a need for selectively passivating GBs in PSCs while keeping the surface of grains intact.[41]

Here, we synthesize and apply biphenyl methylammonium halides (4-phenylbenzylammonium halides, to be exact) and show that they selectively reside on defective sites at the surface, primarily targeting GBs. We attribute this behavior of biphenyl moieties to the two benzene rings offering higher electron cloud density (and hence stronger tendency to passivation)[42] and higher hydrophobicity (and hence greater stability against moisture) than PEAI.[43] This approach also increases charge carrier lifetime by a factor of ~3, resulting in a PCE of 21%, all made in ambient air, with a significant extension of shelf life and operational stabilities.

RESULTS AND DISCUSSION

Device structure

Following our ongoing interests in the ambient air fabrication of stable PSCs,[44] we turned our attention to surface passivation of perovskite. We studied the effect of BiPhX passivation on planar PSCs with an architecture of glass/indium tin oxide (ITO)/tin oxide (SnO_2)/perovskite ($FA_{0.95}MA_{0.05}PbI_{2.85}Br_{0.15}$)/BiPhX/spiro-OMeTAD/Au (Figure 1A), the fabrication of which we reported in detail in our previous work.[44]

EFFECT OF BiPhX INTERLAYER

We first studied the effect of different counter ions to biphenyl methylammonium cation on perovskite photovoltaic performance. We synthesized iodide, bromide, and chloride (referred to as BiPhI, BiPhBr, and BiPhCl, respectively) salts of BiPhX, dissolved in anhydrous 2-propanol in 2 mg mL^{-1} concentration, and spin coated on top of perovskite films (all made in ambient air). We did not synthesize fluoride salt due to safety concerns as it requires the use of highly corrosive hydrofluoric acid (HF). Moreover, traces of HF residue can lead to rougher surfaces and may penetrate through thin films to damage electron transport layer (ETL) or ITO.[45]

We found that BiPhI-treated films had better photovoltaic performance than the control, BiPhBr-, and BiPhCl-treated ones (Figure S1). X-ray diffraction (XRD) analysis revealed that BiPhCl and BiPhBr shifted the perovskite diffraction peak indicative of halide exchange and/or of structural strain in perovskite after passivation.[46] But BiPhI-treated films showed no observable changes on perovskite diffraction pattern (Figure S2), indicating intact perovskite structure. Therefore, we chose BiPhI as a candidate for surface passivation.

We then varied the concentration of BiPhI in 2-propanol and found that 2 mg ml^{-1} was the optimum concentration (Figure S3). At this optimized concentration, the deposited BiPhI layer on perovskite is thick enough to passivate surface defects and thin enough to avoid disturbance of charge transport. A further increase in BiPhI

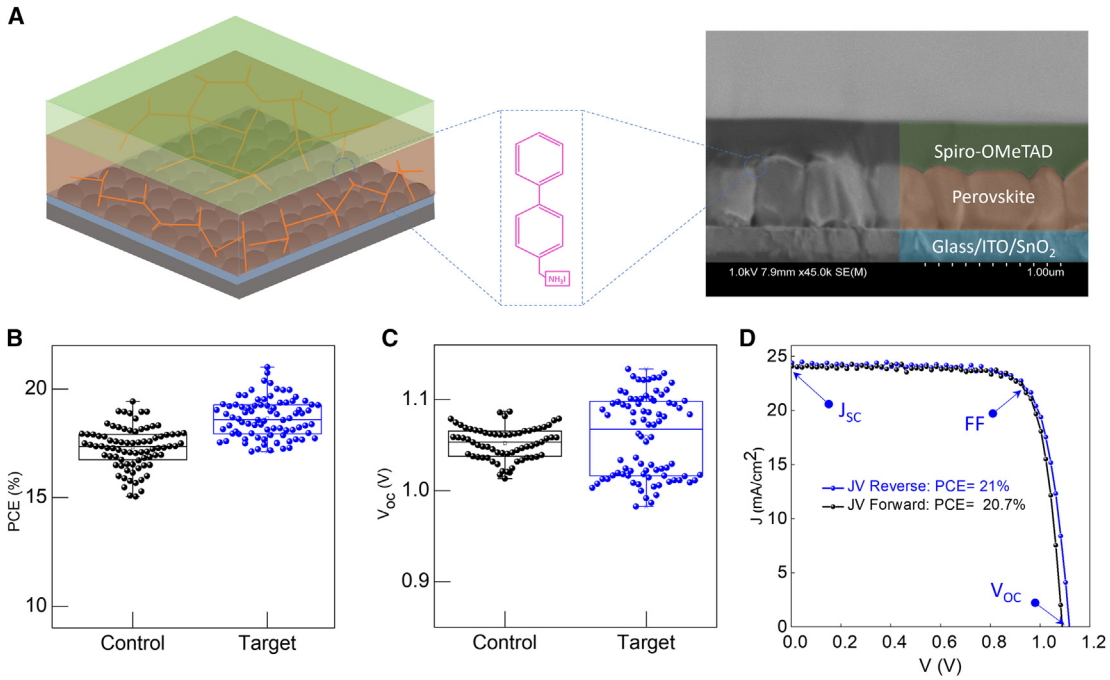

Figure 1. Perovskite solar cells structure and performance

(A) Schematic (left) and cross-sectional SEM image (right) of a typical cell with an architecture of glass/ITO/SnO_2/perovskite/BiPhI/spiro-OMeTAD/Au (note that Au is not seen in these images). The middle panel shows the chemical structure of biphenyl methylammonium iodide.

(B and C) Power conversion efficiency (B) and open-circuit voltage (V_{oc}) (C) of 84 independent perovskite solar cells with and without BiPhI passivation layer. The boxes indicate the 25th and 75th percentiles. The whiskers indicate the minimum and maximum values. The mean value is represented by an open square symbol.

(D) Current-voltage characteristic of a champion target cell.

concentration results in poor device performance (mainly fill factor) due to excessive accumulation of insulating phenyl moieties.[47]

Next, we studied the effect of post-annealing (after BiPhI deposition) on device performance. The results show that the un-annealed films after BiPhI deposition perform better than the annealed ones (Figure S4). This observation agrees with an earlier finding of enhanced stability of PSCs with two-dimensional perovskite layers formed at room temperature with oleylammonium iodide molecules.[48] The higher device efficiency of un-annealed devices could be attributed to better band alignment, resulting in efficient charge transfer at the perovskite-HTL interface (HTL stands for hole transport layer).

Figure 1B shows the statistical data of 84 fabricated devices modified with optimized parameters for BiPhI (2 mg mL^{-1} concentration and without post-annealing). The data show the reproducibility of the devices with mean efficiency of 19% and a consistently enhanced open-circuit voltage over 1 V (Figure 1C). Figure 1D exhibits the JV curve of the champion device with 21% PCE.

To probe the presence of BiPhI on perovskite film, we carried out XRD of both control and target films (Figure 2A). The perovskite's sharp diffraction peak at ~14.1° is observed in both films. However, a new peak at a diffraction angle of 4.7° is observed in the XRD spectra of target film only that cannot be attributed to BiPhI (BiPhI shows a diffraction peak at 4.2°, Figure S2D). To understand the origin of the diffraction peak at 4.7° on perovskite, we carried out a control experiment: we

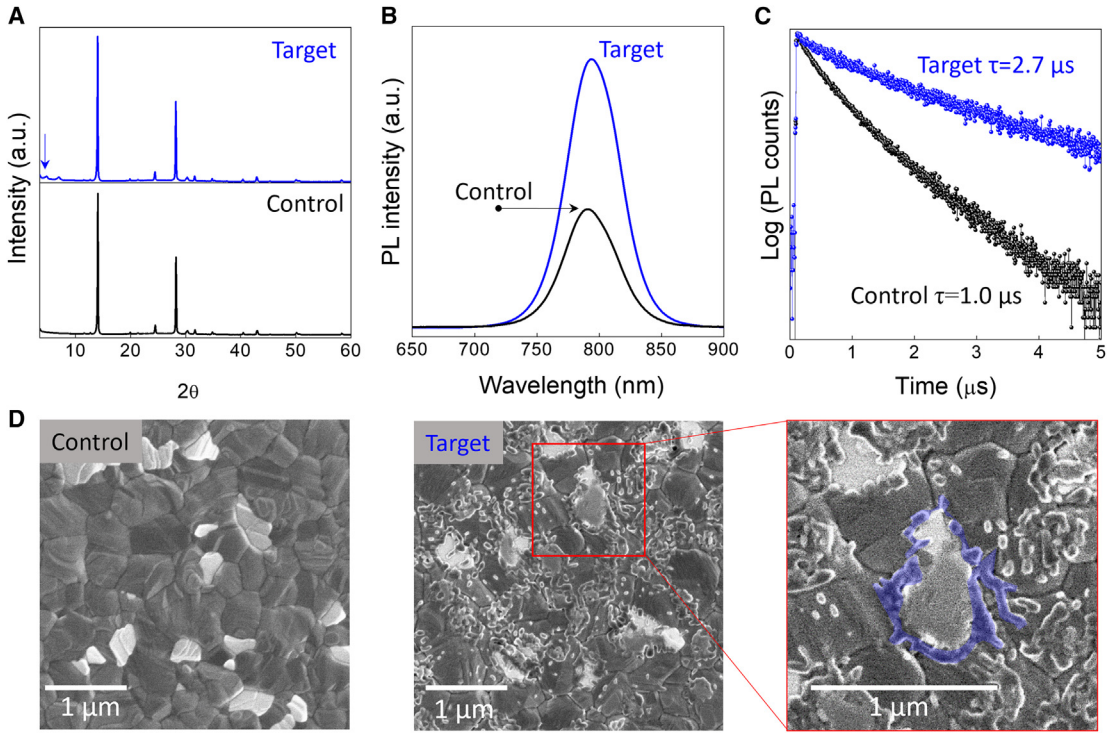

Figure 2. Characterization of both control and target films

(A–D) XRD patterns (A), steady-state photoluminescence spectra (B), time-resolved photoluminescence decay traces (C) at 790 nm, and scanning electron microscope (SEM) images (D) of films. Target film shows selective passivation of grain boundaries. Blue-shaded area is a guide for eyes highlighting spatial distribution of passivating material.

prepared 1 M solution of BiPhI and PbI_2 in 2:1 ratio, respectively, in dimethylformamide (DMF), spin coated on a glass substrate. This product showed a diffraction angle of 4.7°, the same location as we observed on perovskite film (Figure S5).

We studied the morphology of the films with a scanning electron microscope (SEM) (Figure 2D). The control films show an obvious presence of unreacted PbI_2 (white grains). After passivation with BiPhI, we observed that while it is present on the grain surfaces, it predominantly resides on the GBs. To understand the origin of this selective behavior of BiPhI, we treated ground $MAPbI_3$ single crystal with BiPhI and observed no reaction between them (Figure S5). In contrast, we observed a complete reaction between BiPhI and PbI_2 (Figure S5). Hence, we conclude that BiPhI selectively passivates GBs because it reacts with PbI_2, which usually exists in GBs, while keeping the surface of perovskite grains intact for intimate connection with the hole transporter layer.

To probe the origin of increase in the V_{oc}, we monitored the steady-state photoluminescence (PL) of both target and control perovskite films. We observed that the PL intensity for the target film was nearly twice as high than the control film (Figure 2B). The PL lifetime of the perovskite film significantly increased from 1.0 to 2.7 μs after treatment with BiPhI (Figure 2C). This increase in PL intensity and radiative recombination lifetime indicates a significant reduction in the carrier losses, hence, increasing the V_{oc}.

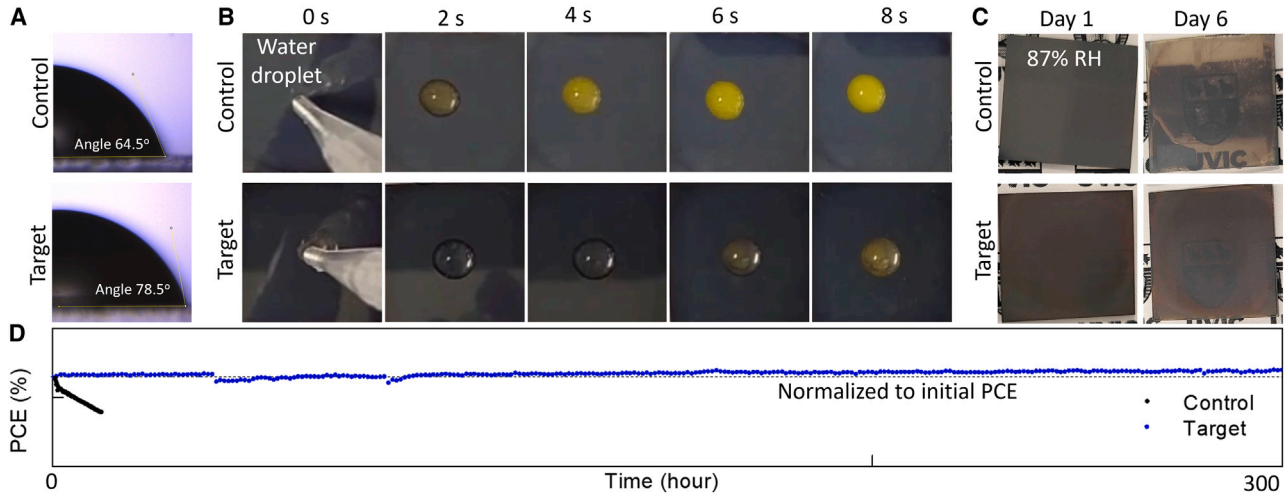

Figure 3. Moisture-tolerance testing of perovskite film and device operational stability

(A) Contact angle between water and perovskite film.

(B) Perovskite film appearance under water droplet (Video S1).

(C) Perovskite film appearance under water vapor.

(E) Operational stability of encapsulated control and target perovskite solar cell.

Film and device stability

We investigated the stability of the control and target films against water. We first conducted the contact angle measurement: the control film showed a sharper angle to water droplets than the target film, indicating the resistance of the target's surface to water/moisture (Figure 3A).

To further confirm this, we directly placed a droplet of water on both control and target films. We observed that the control film shows an obvious sign of degradation in less than a second; however, the target film shows resistance against water and degrades in at least three times longer time (Figure 3B and Video S1).

We then conducted a humidity test of the films. Both control and target films were placed in a container having ~87% relative humidity (RH): we observed significant discoloration of the control film after 6 days under these conditions, while the target film remained almost intact within this period (Figure 3C).

We also tested the stability of both the control and target encapsulated devices at maximum power point (MPP) operation (Figure 3D) at room temperature and RH of 25%–35%. The target device showed a gradual increase in device performance over time, indicating that the use of BiPhI creates a robust interface with the HTL. In contrast, the control device lost >30% of its initial efficiency in 25 h, while the target device remained stable for >300 h. This stability enhancement can be attributed to suppression of ion migration through the perovskite-HTL interface due to surface passivation[49] as well as chemical inertness of biphenyl methylammonium lead iodide, as we discuss below.

To understand the origin of improved stability against moisture, we synthesized biphenyl methylammonium lead iodide single crystals from BiPhI and PbI_2 in hydroiodide acid solvent (see experimental procedures for details). The structure of the crystal was identified by single-crystal XRD (see Data S1). This compound crystallized in monoclinic symmetry, C1 2/c 1 space group, with a brutto-formula of (C_6H_5-C_6H_4-

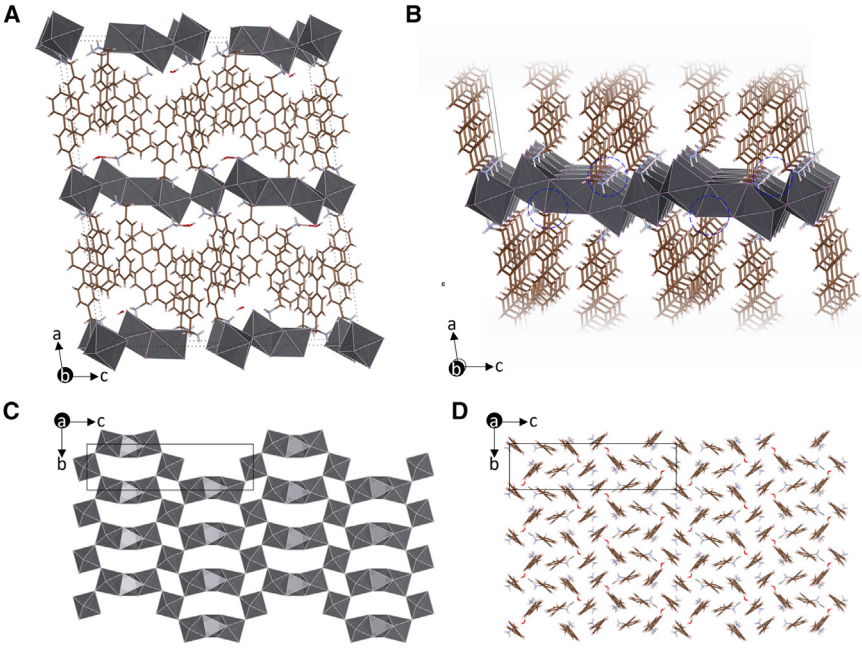

Figure 4. Crystal structure of $(C_6H_5\text{-}C_6H_4\text{-}CH_2\text{-}NH_3)_3Pb_2I_7.H_2O$

(A) Projection of the crystal structure on *ac* crystallographic plane.

(B) The same as (A) with a focus on interaction of organic and inorganic motifs.

(C and D) Inorganic (C) and organic (D) sublattice of the crystal structure.

$CH_2\text{-}NH_3)_3Pb_2I_7.H_2O$, in a two-dimensional pattern, with alternating organic and inorganic layers (Figure 4A). The organic layer is made of $C_6H_5\text{-}C_6H_4\text{-}CH_2\text{-}NH_3^+$ ligands, resembling an edge-to-face herringbone motif of benzene, indicating in-layer π-π interaction (Figure 4D).[50] The inorganic layer is made of trimers of PbI_6 octahedra (face and edge shared) connected through corners of PbI_6 (Figure 4C). When zoomed in, one can clearly observe interpenetration of organic and inorganic sublattices (Figure 4B), indicating strong interaction between the two. This is different from conventional 2D perovskites (e.g., phenethyl ammonium lead iodide), in which the octahedra are only corner shared, and the two sublattices remain spatially separate and hence prone to disintegrate (i.e., decompose). The biphenyl methylammonium lead iodide's π-π interaction within organic sublattice and the inter-penetrating nature of inorganic and organic sublattices explain its inertness against water. In another control experiment, we indeed found that the ground crystal of biphenyl methylammonium lead iodide does not dissolve in water (Figure S6).

In summary, we synthesized and employed BiPhI ligand to selectively passivate perovskite GBs. The presence of double benzene rings in BiPhI enabled strong passivation of the defects and increases hydrophobicity of the surfaces. PL lifetime results showed an increased lifetime of treated perovskite films from 1.0 to 2.7 μs implying the suppression of non-radiative recombination resulting in increased V_{oc}. The target perovskite film showcased improved resistance to moisture. This increased resistance is attributed to the interpenetration of organic and inorganic sublattices in the crystal structure of biphenyl methylammonium lead iodide. The PCE of 21% was achieved, with more than 300 h of device stability at MPP. Our work shows a case for the choice of passivation materials to selectively interact

with defective sites while keeping the grains intact and for the design of crystal structure to increase the chemical inertness of the ultimate functional material.

EXPERIMENTAL PROCEDURES

Resource availability

Lead contact

Further information and requests for resources should be directed to and will be fulfilled by the lead contact, Makhsud I. Saidaminov (msaidaminov@uvic.ca).

Materials availability

The materials synthesized in this work are described in detail in the materials section. More details can be obtained from lead contact upon a reasonable request.

Data and code availability

The authors declare that the experimental data discussed in the work here can be found in the paper and the supplemental information. All other data can be obtained from the lead contact upon reasonable request. The crystallographic information file is deposited in the Cambridge Crystallographic Data Center (CCDC) under deposition number 2260262.

Materials

ITO-coated glass substrates were purchased from Shang Yang Solar (X07-10A). Tin (IV) oxide (SnO_2) 15% in H_2O colloidal dispersion solution was purchased from the Alfa Aesar. Formamidinium iodide (FAI, >99.99%), methylammonium chloride (MACl, >99.99%), and methylammonium bromide (MABr, >99.99%) were purchased from Greatcell Solar Materials, lead (II) iodide (PbI_2, 99.99%) from TCI chemicals, and lead bromide ($PbBr_2$) was purchased from Alfa Aesar. N, N-dimethyl formamide (DMF, 99.5%), dimethyl sulfoxide (DMSO, 99.5%), chlorobenzene (99.5%), and acetonitrile (ACN, $\geq$99.9%) were parched from Milipore Sigma. Sprio-OMeTAD was purchased from Xi'an Polymer Light Technology Co. Bis(trifluoromethane)sulfonimide lithium salt (Li-TFSI 99.95%), 4-*tert*-butylpyridine (tBP, 98%), and cobalt salt (FK 209 Co (III) TFSI) were purchased from Millipore Sigma.

Synthesis of BiPhX

For BiPhI, 15 g of 4-phenylbenzylamine and 50 mL 95% ethanol were added to a 250 mL round-bottom flask and put in an ice bath. Then 7.4 mL of HI solution was added slowly over 30 min using a dripping funnel while under continuous stirring. After complete addition, the mixture was stirred for another 2 h to maximize the yield. The solvent was then evaporated, and the resulting solid was dissolved in a minimum amount of boiling ethanol. After complete dissolution, the solution was left undisturbed overnight for crystallization. The white BiPhMAI solid crystals were filtered out and washed with diethyl ether and dried under vacuum for more than 24 h. The same procedure was followed to prepare BiPhCl and BiPhBr except hydrochloric acid (HCl) and hydrobromic acid (HBr) were used respectively.

Control experiments

To study reaction between PbI_2 and BiPhI, the powders were mixed in 2:1 M ratio and ground together to get the XRD patterns. For the thin films, 1 M solution was prepared in DMF and spin coated on a glass substrate.

To prepare BiPh-PbI_2 single crystals, we dissolved 1 mol of 4-phenylbenzylamine in hot HI acid (on hotplate at ~140°C). Then, we dissolved 1 mol of lead acetate in 5 mL of HI acid. We then added this solution to the precursor solution of 4-phenylbenzylamine and stirred it until it was dissolved. We then slowly cooled the reaction system and observed crystals after ~24 h.

Preparation of solutions

A 7 mL solution of SnO_2 was prepared by taking 6 mL of deionized (DI) water and 1 mL of SnO_2 15% in H_2O colloidal dispersion nanoparticles with a 6:1 volume ratio. It was sonicated for 30 min and filtered with 0.45 μm polyvinylidene difluoride (PVDF) syringe filter before deposition. Perovskite solution based on $FA_{0.95}MA_{0.05}PbI_{2.85}Br_{0.15}$ was prepared by dissolving 217 mg of FAI, 582.7 mg of PbI_2, 7.1 mg of $PbBr_2$, 22 mg of MACl, and 23.3 mg of MABr in 0.8 mL of DMF and 0.1 mL of DMSO. BiPhI solution was prepared by dissolving it in anhydrous isopropyl alcohol (IPA) for 2 mg/mL concentration. Spiro solution was prepared by dissolving 0.1 g of spiro-OMeTAD powder in 1.1 mL of chlorobenzene, 0.039 mL of tBP, 0.023 mL of Li-TFSI (pre-dissolved in acetonitrile, 540 mg/mL), and 0.01 mL of Co-complex (pre-dissolved in acetonitrile, 376 mg/mL) solution. All solutions, i.e., perovskite, biphenyliodide, and spiro-OMeTAD, were filtered with 0.22 μm polytetrafluoroethylene (PTFE) syringe filter.

Device fabrication

Glass substrates were sonicated with DI water, acetone, and isopropanol, respectively, for 15 min. Then, they were dried with a N_2 gas gun and were given ozone treatment for ~15 min. 0.15 mL of already prepared SnO_2 solution was spin coated at 3,000 rpm for 30 s. All the films were then thermally annealed at 150°C for 30 min and again given ozone treatment for 30 min. A perovskite solution of 75 μL was spin coated in a three-step process on top of SnO_2 and thermally annealed for 10 min for crystallization assisted with dripping of diethyl ether in a 3rd step. After that, 0.1 mL of BiPhI solution was spin coated on top of cooled perovskite film at 5,000 rpm for 30 s. A 75 μL solution of spiro-OMeTAD was deposited with a dynamic spin coating method at 2000 rpm for 30 s. A thin layer of ~80 nm of gold was then evaporated on top of the film for front metal connections.

Solar cell characterization

Photovoltaic parameters were measured with Newport Oriel sol-3A (class AAA) solar simulator at standard 1.5 A.M. solar irradiance, and a commercial-grade Si solar cell was used as a reference. The data were recorded with Ossila source meter by scanning the cell from −0.100 to 1.2 V for 0.0907 cm^2 active area at room temperature. Similarly, for operational stability measurements, PSCs were placed in a self-designed LED simulator, and data were recorded with an Ossila source meter with time interval of 15 min between each measurement.

Material characterization

PSCs were fabricated in the air. XRD measurements were done with a PANalytical Empyrean system using a Cu (Kα, 1.5406 Å) source.

SEM images were obtained with a Hitachi S-4800 FESEM. PL spectroscopy was carried out by UV-Vis AVENTES spectrometer (AvaSpec-ULS2048CL-EVO-RS) in the reflection mode ranging from 500 to 780 nm in a dark room every 2 s. Time-resolved photoluminescence (TRPL) measurements were performed on an Edinburgh Instruments OB920 Single Photon Counting system. The samples were

excited using a 510-nm pulsed laser diode. Emission was collected at 780 nm using a 16-nm bandwidth monochromator.

For single-crystal XRD, a crystal was coated in paratone oil, mounted on a MiTeGen Micro Mount, and transferred to the cold stream (150 K) of the X-ray diffractometer. Data were collected on a Bruker Smart instrument equipped with an APEX II CCD area detector fixed at 5.0 cm from the crystal and a Cu Kα fine-focus sealed tube (λ = 1.54178 nm) operated at 1.5 kW (50 kV, 30 mA), filtered with a graphite monochromator. Data were collected at 173 K; the temperature was regulated using an Oxford Cryosystems Cryostream 700.

SUPPLEMENTAL INFORMATION

Supplemental information can be found online at https://doi.org/10.1016/j.xcrp.2023.101634.

ACKNOWLEDGMENTS

We thank Solaires Entreprises Inc. and Canada's Natural Sciences and Engineering Research Council (ALLRP 561355-20) for their financial support. M.I.S. is grateful to the NSERC (RGPIN-2020-04239), the Canada Research Chairs Program (CRC-2019-00297), the Canadian Foundation for Innovation (40326), and B.C. Knowledge Development Fund (806169) for operational and infrastructure support.

AUTHOR CONTRIBUTIONS

Conceptualization, M.A. and S.K.; investigation, M.A., S.K., D.Y., V.Y., and M.R.K.; resources, M.I.S.; writing – original draft, M.A.; writing – review and editing, M.I.S., F.T., S.D., S.K., W.Z., and Y.A.; supervision, M.I.S. M.A. and S.K. contributed equally to this work.

DECLARATION OF INTERESTS

The authors declare no competing interests.

Received: May 19, 2023
Revised: August 30, 2023
Accepted: September 19, 2023
Published: October 9, 2023

REFERENCES

1. Kojima, A., Teshima, K., Shirai, Y., and Miyasaka, T. (2009). Organometal halide perovskites as visible-light sensitizers for photovoltaic cells. J. Am. Chem. Soc. *131*, 6050–6051. https://doi.org/10.1021/ja809598r.

2. Lee, M.M., Teuscher, J., Miyasaka, T., Murakami, T.N., and Snaith, H.J. (2012). Efficient hybrid solar cells based on meso-superstructured organometal halide perovskites. Science (1979 *338*, 643–647. https://doi.org/10.1126/science.1228604.

3. Burschka, J., Pellet, N., Moon, S.-J., Humphry-Baker, R., Gao, P., Nazeeruddin, M.K., and Grätzel, M. (2013). Sequential deposition as a route to high-performance perovskite-sensitized solar cells. Nature *499*, 316–319. https://doi.org/10.1038/nature12340.

4. Im, J.H., Lee, C.R., Lee, J.W., Park, S.W., and Park, N.G. (2011). 6.5% efficient perovskite quantum-dot-sensitized solar cell. Nanoscale *3*, 4088–4093. https://doi.org/10.1039/C1NR10867K.

5. Awais, M., Kirsch, R.L., Yeddu, V., and Saidaminov, M.I. (2021). Tin Halide Perovskites Going Forward: Frost Diagrams Offer Hints. ACS Mater. Lett. *3*, 299–307. https://doi.org/10.1021/acsmaterialslett.0c00571.

6. Tailor, N.K., Kar, S., Mishra, P., These, A., Kupfer, C., Hu, H., Awais, M., Saidaminov, M., Dar, M.I., Brabec, C., and Satapathi, S. (2021). Advances in Lead-Free Perovskite Single Crystals: Fundamentals and Applications. ACS Mater. Lett. *3*, 1025–1080. https://doi.org/10.1021/acsmaterialslett.1c00242.

7. Ahmed, Y., Khan, B., Bilal Faheem, M., Huang, K., Gao, Y., and Yang, J. (2022). Organic additives in all-inorganic perovskite solar cells and modules: from moisture endurance to enhanced efficiency and operational stability. J. Energy Chem. *67*, 361–390. https://doi.org/10.1016/j.jechem.2021.09.047.

8. Liu, D., Zheng, H., Ahmed, Y., Zheng, C., Wang, Y., Chen, H., Chen, L., and Li, S. (2022). Enhanced photovoltaic performance of SnO2 based flexible perovskite solar cells via introducing interfacial dipolar layer and defect passivation. J. Power Sources *519*, 230814. https://doi.org/10.1016/j.jpowsour.2021.230814.

9. Aldamasy, M., Iqbal, Z., Li, G., Pascual, J., Alharthi, F., Abate, A., and Li, M. (2021). Challenges in tin perovskite solar cells. Phys. Chem. Chem. Phys. *23*, 23413–23427. https://doi.org/10.1039/D1CP02596A.

10. Ullah, A., Park, K.H., Lee, Y., Park, S., Faheem, A.B., Nguyen, H.D., Siddique, Y., Lee, K.K., Jo, Y., Han, C.H., et al. (2022). Versatile Hole Selective Molecules Containing a Series of

Heteroatoms as Self-Assembled Monolayers for Efficient p-i-n Perovskite and Organic Solar Cells. Adv. Funct. Mater. *32*, 2208793. https://doi.org/10.1002/adfm.202208793.

11. Xu, B., Liu, D., Dong, C., Awais, M., Wang, W., Song, Y., Deng, Y., Yao, M., Tong, J., Yue, G., et al. (2023). NiOx for interface and work function engineering in carbon-based all-inorganic perovskite solar cells. J. Colloid Interface Sci. *641*, 105–112. https://doi.org/10.1016/j.jcis.2023.03.049.

12. Finkenauer, B.P., Gao, Y., Wang, X., Tian, Y., Wei, Z., Zhu, C., Rokke, D.J., Jin, L., Meng, L., Yang, Y., et al. (2021). Mechanically robust and self-healable perovskite solar cells. Cell Rep. Phys. Sci. *2*, 100320. https://doi.org/10.1016/j.xcrp.2020.100320.

13. Wang, H.Q., Wang, S., Chen, L., Yin, Z., Mei, S., Zhong, Y., Yao, Y., Li, N., Wang, J., and Song, W. (2021). Understanding degradation mechanisms of perovskite solar cells due to electrochemical metallization effect. Sol. Energy Mater. Sol. Cell. *230*, 111278. https://doi.org/10.1016/j.solmat.2021.111278.

14. Liu, J., Pathak, S.K., Sakai, N., Sheng, R., Bai, S., Wang, Z., and Snaith, H.J. (2016). Identification and Mitigation of a Critical Interfacial Instability in Perovskite Solar Cells Employing Copper Thiocyanate Hole-Transporter. Adv. Mater. Interfaces *3*, 1600571. https://doi.org/10.1002/admi.201600571.

15. Leijtens, T., Eperon, G.E., Pathak, S., Abate, A., Lee, M.M., and Snaith, H.J. (2013). Overcoming ultraviolet light instability of sensitized TiO2 with meso-superstructured organometal tri-halide perovskite solar cells. Nat. Commun. *4*, 2885–2888. https://doi.org/10.1038/ncomms3885.

16. Khenkin, M.v., Katz, E.A., Abate, A., Bardizza, G., Berry, J.J., Brabec, C., Brunetti, F., Bulović, V., Burlingame, Q., di Carlo, A., et al. (2020). Consensus statement for stability assessment and reporting for perovskite photovoltaics based on ISOS procedures. Nat. Energy *5*, 35–49. https://doi.org/10.1038/s41560-019-0529-5.

17. Yoo, J.J., Seo, G., Chua, M.R., Park, T.G., Lu, Y., Rotermund, F., Kim, Y.K., Moon, C.S., Jeon, N.J., Correa-Baena, J.P., et al. (2021). Efficient perovskite solar cells via improved carrier management. Nature *590*, 587–593. https://doi.org/10.1038/s41586-021-03285-w.

18. Nazir, G., Lee, S.-Y., Lee, J.-H., Rehman, A., Lee, J.-K., Seok, S.I., and Park, S.-J. (2022). Stabilization of Perovskite Solar Cells: Recent Developments and Future Perspectives. Adv. Mater. *34*, 2204380. https://doi.org/10.1002/adma.202204380.

19. Fu, W., Ricciardulli, A.G., Akkerman, Q.A., John, R.A., Tavakoli, M.M., Essig, S., Kovalenko, M.V., and Saliba, M. (2022). Stability of perovskite materials and devices. Mater. Today *58*, 275–296. https://doi.org/10.1016/j.mattod.2022.06.020.

20. Quan, L.N., Rand, B.P., Friend, R.H., Mhaisalkar, S.G., Lee, T.W., and Sargent, E.H. (2019). Perovskites for Next-Generation Optical Sources. Chem. Rev. *119*, 7444–7477. https://doi.org/10.1021/acs.chemrev.9b00107.

21. Kundu, S., Zhang, D., Askar, A.M., Moloney, E.G., Adachi, M.M., Nadeem, A., Moradi, S., Yeddu, V., Abdelhady, A.L., Voznyy, O., and Saidaminov, M.I. (2022). Bismuth Stabilizes the α-Phase of Formamidinium Lead Iodide Perovskite Single Crystals. ACS Mater. Lett. *4*, 707–712. https://doi.org/10.1021/acsmaterialslett.1c00778.

22. Wang, S., Cabreros, A., Yang, Y., Hall, A.S., Valenzuela, S., Luo, Y., Correa-Baena, J.P., Kim, M.c., Fjeldberg, Ø., Fenning, D.P., and Meng, Y.S. (2020). Impacts of the Hole Transport Layer Deposition Process on Buried Interfaces in Perovskite Solar Cells. Cell Rep. Phys. Sci. *1*, 100103. https://doi.org/10.1016/j.xcrp.2020.100103.

23. Wu, Z., Alsalloum, A.Y., Mohammed, O.F., Bakr, O.M., Duan, L., Duan, D.P., and Yang, J.S. (2022). Soft perovskites stabilized by robust heterojunctions. Joule *6*, 951–952. https://doi.org/10.1016/j.joule.2022.04.015.

24. Hou, Y., Du, X., Scheiner, S., McMeekin, D.P., Wang, Z., Li, N., Killian, M.S., Chen, H., Richter, M., Levchuk, I., et al. (2017). A generic interface to reduce the efficiency-stability-cost gap of perovskite solar cells. Science *358*, 1192–1197. https://doi.org/10.1126/science.aao5561.

25. Wu, T., Qin, Z., Wang, Y., Wu, Y., Chen, W., Zhang, S., Cai, M., Dai, S., Zhang, J., Liu, J., et al. (2021). The Main Progress of Perovskite Solar Cells in 2020–2021. Nano-Micro Lett. *13*, 1–18. https://doi.org/10.1007/s40820-021-00672-w.

26. Babics, M., De Bastiani, M., Ugur, E., Xu, L., Bristow, H., Toniolo, F., Raja, W., Subbiah, A.S., Liu, J., Torres Merino, L.V., et al. (2023). One-year outdoor operation of monolithic perovskite/silicon tandem solar cells. Cell Rep. Phys. Sci. *4*, 101280. https://doi.org/10.1016/j.xcrp.2023.101280.

27. Mali, S.S., Patil, J.V., Park, D.W., Jung, Y.H., and Hong, C.K. (2022). Intrinsic and extrinsic stability of triple-cation perovskite solar cells through synergistic influence of organic additive. Cell Rep. Phys. Sci. *3*, 100906. https://doi.org/10.1016/j.xcrp.2022.100906.

28. Ka, I., Asuo, I.M., Nechache, R., and Rosei, F. (2021). Highly stable air processed perovskite solar cells by interfacial layer engineering. Chem. Eng. J. *423*, 130334. https://doi.org/10.1016/j.cej.2021.130334.

29. Byranvand, M.M., and Saliba, M. (2021). Defect Passivation of Perovskite Films for Highly Efficient and Stable Solar Cells. Sol. RRL *5*, 2100295. https://doi.org/10.1002/solr.202100295.

30. Lu, H., Krishna, A., Zakeeruddin, S.M., Grätzel, M., and Hagfeldt, A. (2020). Compositional and Interface Engineering of Organic-Inorganic Lead Halide Perovskite Solar Cells. iScience *23*, 101359. https://doi.org/10.1016/j.isci.2020.101359.

31. Jeon, N.J., Noh, J.H., Yang, W.S., Kim, Y.C., Ryu, S., Seo, J., and Seok, S.I. (2015). Compositional engineering of perovskite materials for high-performance solar cells. Nature *517*, 476–480. https://doi.org/10.1038/nature14133.

32. Jiang, Q., Zhao, Y., Zhang, X., Yang, X., Chen, Y., Chu, Z., Ye, Q., Li, X., Yin, Z., and You, J. (2019). Surface passivation of perovskite film for efficient solar cells. Nat. Photonics *13*, 460–466. https://doi.org/10.1038/s41566-019-0398-2.

33. Zheng, X., Chen, B., Dai, J., Fang, Y., Bai, Y., Lin, Y., Wei, H., Zeng, X., and Huang, J. (2017). Defect passivation in hybrid perovskite solar cells using quaternary ammonium halide anions and cations. Nat. Energy *2*, 1–9. 17102. https://doi.org/10.1038/nenergy.2017.102.

34. Fakharuddin, A., Schmidt-Mende, L., Garcia-Belmonte, G., Jose, R., and Mora-Sero, I. (2017). Interfaces in Perovskite Solar Cells. Adv. Energy Mater. *7*, 1700623. https://doi.org/10.1002/aenm.201700623.

35. Li, X., Dar, M.I., Yi, C., Luo, J., Tschumi, M., Zakeeruddin, S.M., Nazeeruddin, M.K., Han, H., and Grätzel, M. (2015). Improved performance and stability of perovskite solar cells by crystal crosslinking with alkylphosphonic acid ω-ammonium chlorides. Nat. Chem. *7*, 703–711. https://doi.org/10.1038/nchem.2324.

36. Castro-Méndez, A.F., Hidalgo, J., and Correa-Baena, J.P. (2019). The Role of Grain Boundaries in Perovskite Solar Cells. Adv. Energy Mater. *9*, 1901489. https://doi.org/10.1002/aenm.201901489.

37. Arabpour Roghabadi, F., Mansour Rezaei Fumani, N., Alidaei, M., Ahmadi, V., and Sadrameli, S.M. (2019). High Power UV-Light Irradiation as a New Method for Defect Passivation in Degraded Perovskite Solar Cells to Recover and Enhance the Performance. Sci. Rep. *9*, 9448. https://doi.org/10.1038/s41598-019-45756-1.

38. Wenson, G., Thakkar, H., Tsai, H., Stein, J., Singh, R., and Nie, W. (2022). The degradation and recovery behavior of mixed-cation perovskite solar cells in moisture and a gas mixture environment. J. Mater. Chem. A Mater. *10*, 13519–13526. https://doi.org/10.1039/D2TA02352K.

39. Kundu, S., and Kelly, T.L. (2020). In situ studies of the degradation mechanisms of perovskite solar cells. EcoMat *2*, e12025. https://doi.org/10.1002/eom2.12025.

40. Frost, J.M., Butler, K.T., Brivio, F., Hendon, C.H., Van Schilfgaarde, M., and Walsh, A. (2014). Atomistic origins of high-performance in hybrid halide perovskite solar cells. Nano Lett. *14*, 2584–2590. https://doi.org/10.1021/nl500390f.

41. Jiao, H., Ni, Z., Shi, Z., Fei, C., Liu, Y., Dai, X., and Huang, J. (2022). Perovskite grain wrapping by converting interfaces and grain boundaries into robust and water-insoluble low-dimensional perovskites. Sci. Adv. *8*, eabq4524. https://doi.org/10.1126/sciadv.abq4524.

42. Qiu, L., Li, H., Dai, F., Ouyang, F., Pang, D., and Wang, H. (2020). Adsorption and photocatalytic degradation of benzene compounds on acidic F-TiO2/SiO2 catalyst. Chemosphere *246*, 125698. https://doi.org/10.1016/j.chemosphere.2019.125698.

43. Kang, Y.J., and Na, S.I. (2022). Multi-site passivation-based antisolvent additive engineering with gradient distribution for superior triple cation P-I-N perovskite solar cells. Nano Energy *97*, 107193. https://doi.org/10.1016/j.nanoen.2022.107193.

44. Awais, M., Thrithamarassery Gangadharan, D., Tan, F., and Saidaminov, M.I. (2022). How to Make 20% Efficient Perovskite Solar Cells in Ambient Air and Encapsulate Them for 500 h of Operational

Stability. Chem. Mater. *34*, 8112–8118. https://doi.org/10.1021/acs.chemmater.2c01422.

45. Hu, A., Lu, T., Chen, D., Huang, J., Feng, W., Li, Y., Guo, D., Xu, X., Chen, D., and Xiong, F. (2019). The effect of boric acid concentration on the TiO_2 compact layer by liquid-phase deposition for dye-sensitized solar cell. BMC Genet. *20*, 7–14. https://doi.org/10.1016/j.apsusc.2018.05.113.

46. Sidhik, S., Wang, Y., de Siena, M., Asadpour, R., Torma, A.J., Terlier, T., Ho, K., Li, W., Puthirath, A.B., Shuai, X., et al. (2022). Deterministic fabrication of 3D/2D perovskite bilayer stacks for durable and efficient solar cells. Science *377*, 1425–1430. https://doi.org/10.1126/science.abq7652.

47. Jiang, X., Chen, S., Li, Y., Zhang, L., Shen, N., Zhang, G., Du, J., Fu, N., and Xu, B. (2021). Direct Surface Passivation of Perovskite Film by 4-Fluorophenethylammonium Iodide toward Stable and Efficient Perovskite Solar Cells. ACS Appl. Mater. Interfaces *13*, 2558–2565. https://doi.org/10.1021/acsami.0c17773.

48. Azmi, R., Ugur, E., Seitkhan, A., Aljamaan, F., Subbiah, A.S., Liu, J., Harrison, G.T., Nugraha, M.I., Eswaran, M.K., Babics, M., et al. (2022). Damp heat-stable perovskite solar cells with tailored-dimensionality 2D/3D heterojunctions. Science (1979) *376*, 73–77. https://doi.org/10.1126/science.abm5784.

49. Li, Q., Zheng, Y., Wei, Z., Xie, J., Zou, C., Liu, X., Liu, D., Zhou, Z., Yang, H.G., Yang, S., and Hou, Y. (2022). Halide diffusion equilibrium and its impact on efficiency evolution of perovskite solar cells. Adv. Energy Mater. *12*, 2202982. https://doi.org/10.1002/aenm.202202982.

50. Nayak, S.K., Sathishkumar, R., and Row, T.N.G. (2010). Directing role of functional groups in selective generation of C–H···π interactions: In situ cryo-crystallographic studies on benzyl derivatives. CrystEngComm *12*, 3112–3118. https://doi.org/10.1039/C001190H.